INTERNATIONAL JOURNAL OF
NUMERICAL ANALYSIS AND MODELING
Volume 23, Number 4, Pages 499–522

doi: 10.4208/ijnam2026-1022

ACCELERATING CONVERGENCE OF A NATURAL CONVECTION SOLVER BY CONTINUOUS DATA ASSIMILATION

ELIZABETH HAWKINS

Abstract. The Picard iteration for the Boussinesq model of natural convection can be an attractive solver because it stably decouples the fluid equations from the temperature equation (for contrast, the Newton iteration does not stably decouple). However, the convergence of Picard for this system is at best linear, but slows as the Rayleigh number increases, eventually failing for even moderately sized Rayleigh numbers. We consider this solver in the setting where sparse solution data is available, e.g. from data measurements or solution observables, and enhance Picard by incorporating the partial solution data into the iteration using a continuous data assimilation (CDA) approach. We prove that our approach scales the linear convergence rate by $H^{\frac{1}{2}}$, with nudging velocity (or both velocity and temperature) producing the best results. This implies that when Picard is converging, CDA will accelerate convergence, and when Picard is not converging, CDA (with enough partial solution data) will *enable* convergence. In the case of noisy partial solution data, we prove that the linear convergence rate of the nonlinear residual is similarly scaled by $H^{\frac{1}{2}}$ but the accuracy is limited by the accuracy of the partial solution data. This is overcome by using CDA-Picard to achieve a specific tolerance for the residual and then switching the solver to Newton. Several numerical tests illustrate the effectiveness of the proposed methods. These tests show that CDA style nudging adapted to an iteration (instead of a time stepping scheme) enables convergence at much higher Rayleigh number.

Key words. Acceleration, Picard iteration, natural convection, continuous data assimilation.

1. Introduction

Fluid flows with varying temperature (or density) can be modeled by the Boussinesq system for non-isothermal flow/natural convection. This multiphysics model can be observed in nature in atmospheric models and katabatic winds, in ventilation design, dense gas dispersion, insulation with double pane window, and solar collectors [12], to just name a few examples. We consider the Boussinesq system on a finite, connected domain $\Omega \subset \mathbb{R}^d$ $(d = 2, 3)$ with boundary $\Gamma_1 \cup \Gamma_2$. We denote u to be the fluid velocity, p is the pressure, T is the temperature (or density), $\nu > 0$ is the kinematic viscosity of the fluid, $\kappa > 0$ the thermal diffusivity, f the external forcing term, and $Ri > 0$ the Richardson number which accounts for the gravitational force and thermal expansion of the fluid. This system is given by

$$\begin{cases} u \cdot \nabla u + \nabla p - \nu \Delta u &= f + Ri\ T\ \bar{e}_d, \text{ in } \Omega, \\ \nabla \cdot u &= 0 \text{ in } \Omega, \\ u \cdot \nabla T - \kappa \Delta T &= g \text{ in } \Omega, \end{cases} \tag{1}$$

where e_d is a unit vector in $\mathbb{R}^d$ where the last element is one. with no-slip boundary conditions for velocity and mixed homogenous Dirichlet and homogenous Neumann

Received by the editors on March 31, 2025 and accepted on January 8, 2026.
2000 *Mathematics Subject Classification.* 65Nxx.

for temperature (the latter of which corresponds to perfect insulation):

$$\begin{cases} u & = 0 \text{ on } \partial\Omega, \\ T & = 0 \text{ on } \partial\Gamma_1, \\ \nabla T \cdot n & = 0 \text{ on } \partial\Gamma_2. \end{cases} \tag{2}$$

The physical constants that the model relies on are expressed as the Reynolds number Re, the Prandtl number Pr, and the Rayleigh number Ra, which are given by

$$Re = \nu^{-1},\ Pr = \frac{\nu}{\kappa},\ Ra = Ri\ Re^2\ Pr.$$

For any set of problem data ($\nu,\ Ri,\ \kappa,\ f,\ g$), the system (1)-(2) is known to admit weak solutions [5]. Under a smallness condition on this problem data, the system is known to be well-posed; for sufficiently high Ra, this system may lose uniqueness [5]. (see Section 2)

The Picard iteration is a common method for solving the system (1)-(2), and is given by

$$\begin{cases} u^k \cdot \nabla u^{k+1} + \nabla p^{k+1} - \nu\Delta u^{k+1} & = f + Ri\ T\ \bar{e}_d, , \\ \nabla \cdot u^{k+1} & = 0, \\ u^k \cdot \nabla T^{k+1} - \kappa\Delta T^{k+1} & = g, \end{cases} \tag{3}$$

together with (2) for u^{k+1} and T^{k+1}. Note that the system equations (3) decouple because the velocity term in the heat transport equation is known. This makes each iteration of Picard efficient since one can first solve for T^{k+1} and then solve an Oseen Problem for u^{k+1} and p^{k+1}. Picard admits stable solutions for any problem data and produces unique solutions provided the problem data satisfies a smallness condition on the problem data (see Section 2). However, this iteration converges linearly for sufficiently small problem data (see Section 2) but the linear convergence rate decreases as Ra increases and fails for even moderate Ra [27, 37].

The purpose of this paper is to improve Picard for the Boussinesq equations in the setting of where partial solution data is available, by incorporating continuous data assimilation (CDA) style nudging into the Picard iteration (a method we will call CDA-Picard). Partial solution data may be available from physical experiments, measurements of physical phenomena, or even from a high resolution simulation where passing all solution data is too expensive. Note that the collected partial solution data could include noise, such as that which occurs from physical measurements.

We have recently shown that CDA ideas help in solving steady Navier-Stokes equations (NSE) using Picard [35, 23], which is perhaps surprising since CDA is designed for continuous in time assimilation. We consider herein a natural extension of this idea to multiphysics problems. Analysis of this type of CDA applied to Boussinesq poses significant extra difficulties and considerations compared to NSE, and it turns out to give some unexpected results. This is because the Boussinesq equations are given by NSE coupled to a heat transport equation, which includes extra nonlinear terms. Furthermore, unlike NSE, Boussinesq has the unknown variable T as well as u thus CDA nudging is applicable to multiple variables. Hence, there are extra cases to consider for CDA applied to the Boussinesq equations: nudging both u and T, nudging just u, and nudging just T.

CDA is performed using an interpolant I_H where H is representative of the spacing of collected partial solution data and $I_H(u)$ and $I_H(T)$ are interpolants of

the partial solution data projected in the solution space. Thus, CDA-Picard for the Boussinesq equations takes the form (together with (2))

$$(4)\qquad \begin{cases} u^k \cdot \nabla u^{k+1} + \nabla p^{k+1} - \nu \Delta u^{k+1} + \mu_1 I_H(u^{k+1} - u) & = f + Ri\ T^{k+1}\ \bar{e}_d, \\ \nabla \cdot u^{k+1} & = 0, \\ u^k \cdot \nabla T^{k+1} - \kappa \Delta T^{k+1} + \mu_2 I_H(T^{k+1} - T) & = g, \end{cases}$$

where $\mu_1 > 0$ and $\mu_2 > 0$ are user chosen nudging constants. For simplicity we restrict (4) to the case where $I_H(u)$ and $I_H(T)$ are data collected at the same locations. Because $I_H(u)$ and $I_H(T)$ may come from collected data it is a natural assumption that the partial solution data includes noise (inaccuracies). This will inevitably affect the convergence and accuracy of CDA-Picard and therefore we investigate this case as well.

CDA was first proposed by Azouani, Olson, and Titi in 2014 [2] for time dependent systems and has since been applied to a wide variety of time dependent problems including NSE and turbulence [2, 32, 21, 7], the Cahn-Hilliard equation [14], planetary geostrophic modeling [20], Benard convection [17], and many others. Interest in CDA has increased in the last decade leading to many improvements to the algorithm and uses for it, such as for sensitivity analyses [15], parameter recovery [8, 9], numerical methods and analyses [28, 30, 34, 14, 24, 29]. Of recent interest is modification to the algorithm such as adaptive nudging [11] and direct enforcement [13]. There have also been several works investigating the use of the algorithm with restrictions on the observational data, including measurement error [4, 10, 22] and partial observations of the problem variables [17, 19, 18, 20].

We prove herein that in the absence of noise in the partial solution data, CDA-Picard has a convergence rate that is improved by a factor of $H^{\frac{1}{2}}$ compared to Picard, when nudging both u and T. We also prove that when nudging just u there is a similar improvement, but not when nudging just T where there is a partial scaling of the convergence rate. This is surprising, since in the time dependent case, it is sufficient to nudge just T to achieve long time accuracy [19]. Note that a partial scaling of the convergence rate is still an improvement (under certain conditions) but just not as much of an improvement as expected. We also prove that CDA-Picard using noisy partial solution data similarly scales the convergence rate of the residual by $H^{\frac{1}{2}}$ and concurrently the limit solution accuracy is bounded by the accuracy of the partial solution data. We find the limit solution of CDA-Picard with noisy partial solution data is typically within the convergence basin of Newton, meaning that a modified method incorporating Newton can overcome the accuracy limitations caused by the noisy partial solution data and provide an effective nonlinear solver.

We remark that while CDA is a tool to utilize available data to gain improved convergence (under certain conditions), it can also be used alongside other nonlinear acceleration techniques without issue such as Anderson acceleration in [35, 33] or preconditioned Newton [25] by using CDA-Picard as the preconditioner in place of Picard. Hence, CDA should not be considered a direct competitor for other nonlinear acceleration techniques but instead should be considered as defining a data-informed variation of the desired method that can converge faster than the original method.

This paper is arranged as follows. First we present notation, and then stability and convergence results for Picard in Section 2. These Picard results are known, and will be important for comparison in the analysis that follows. Then we give analysis in Section 4 for CDA-Picard when nudging both u and T, just u, and just T. Section

5 considers these same questions as Section 4 but with noisy partial solution data. In Section 6 we apply the proposed methods to $2D$ and $3D$ benchmark problem both with and without noise, and propose a modification of CDA-Picard with noisy partial solution data to incorporate Newton.

2. Preliminaries

Let $\Omega \subset \mathbb{R}^d$ ($d = 2$ or 3) be a connected domain with boundary $\partial\Omega = \Gamma_1 \cup \Gamma_2$ satisfying $meas(\Gamma_1 \cap \Gamma_2) = 0$. Let $(\cdot,\cdot)$ and $\|\cdot\|$ denote the $L^2(\Omega)$ inner product and $L^2(\Omega)$ norm, respectively. We define the pressure, temperature, velocity and divergence free velocity solution spaces as

$$\begin{aligned} Q &= \left\{ q \in L^2(\Omega) : \int_\Omega q \; d\Omega = 0 \right\}, \\ D &= \left\{ S \in H^1(\Omega) : S|_{\Gamma_1} = 0 \right\}, \\ X &= \left\{ v \in H^1 : v|_{\partial\Omega} = 0 \right\}, \\ V &= \left\{ v \in X : (\nabla \cdot v, q) = 0 \; \forall q \in Q \right\}. \end{aligned}$$

Let X^*, V^*, and D^* represent the dual spaces of X, V, and D, respectively. We use $(\cdot,\cdot)$ to also denote the dual pairings of these spaces. For $z \in X,\ V,$ or D, it is known that the Poincaré inequality holds:

$$\|z\| \le C_p \|\nabla z\|,$$

where $C_p > 0$ is a constant depending only on Ω.

Let $b : X \times X \times X \to \mathbb{R}$ and $\hat{b} : X \times D \times D \to \mathbb{R}$ denote the trilinear functionals given by:

$$\begin{aligned} b(u,v,w) &:= (u \cdot \nabla v, w) + \frac{1}{2}((\nabla \cdot u)v, w), \\ \hat{b}(u,v,w) &:= (u \cdot \nabla s, t) + \frac{1}{2}((\nabla \cdot u)s, t). \end{aligned}$$

These trilinear functionals defined above are skew-symmetric,

$$b(u,v,v) = 0 \text{ and } \hat{b}(u,s,t) = 0.$$

We will bound b and $\hat{b}$ herein using the well known bounds [31]: $\forall u, v, w \in X$, $s, t \in D$, $\exists C_s > 0$ depending only on $|\Omega|$ such that

$$|b(u,v,w)| \le C_s \|\nabla u\| \|\nabla v\| \|w\|^{1/2} \|\nabla w\|^{1/2}, \tag{5}$$

$$|\hat{b}(u,s,t)| \le C_s \|\nabla u\| \|\nabla s\| \|t\|^{1/2} \|\nabla t\|^{1/2}, \tag{6}$$

and

$$|b(u,v,w)| \le C_p^{1/2} C_s \|\nabla u\| \|\nabla v\| \|\nabla w\|, \tag{7}$$

$$|\hat{b}(u,s,t)| \le C_p^{1/2} C_s \|\nabla u\| \|\nabla s\| \|\nabla t\|. \tag{8}$$

2.1. Boussinesq preliminaries. The system (1)-(2) is known to admit stable solutions for any $Ra > 0$ [5], which can be proven similarly to the analogous result for the steady NSE by using the Leray-Schauder theorem. However, uniqueness for (9) requires a smallness condition on the problem data. These results are provided below and we give the proofs for the following results in the appendix for completeness.

The Galerkin weak formulation of the Boussinesq equations takes the form: Given $f \in X^*$ and $g \in D^*$, find $(u, p, T) \in X \times Q \times D$ satisfying $\forall (v, q, w) \in (X \times Q \times D)$

$$\begin{cases} b(u,u,v) - (p, \nabla \cdot v) + \nu(\nabla u, \nabla v) & = (f,v) + Ri(T\ \bar{e}_d, v), \\ (\nabla \cdot u, q) & = 0, \\ \hat{b}(u,T,w) + \kappa(\nabla T, \nabla w) & = (g,w). \end{cases}$$

Note that the perfect insulation condition $\nabla T \cdot n|_{\Gamma_2}$ is weakly enforced. The spaces $X, Q,$ and D satisfy an LBB condition. Therefore the problem can be reformulated using V as: Given $f \in V^*$ and $g \in D^*$, find $(u, T) \in V \times D$ satisfying for all $(v, w) \in V \times D$

$$\begin{cases} b(u,u,v) + \nu(\nabla u, \nabla v) & = (f,v) + Ri(T\ \bar{e}_d, v), \\ \hat{b}(u,T,w) + \kappa(\nabla T, \nabla w) & = (g,w). \end{cases} \tag{9}$$

Lemma 2.1. Any solution to the Boussinesq equations (9) satisfies the a priori estimate

$$\|\nabla T\| \leq \|\nabla T\| \leq \kappa^{-1} \|g\|_{D^*} =: M_2, \tag{10}$$

$$\|\nabla u\| \leq \|\nabla u\| \leq \nu^{-1} \|f\|_{V^*} + Ri C_p^2 \nu^{-1} M_2 =: M_1. \tag{11}$$

Lemma 2.2. Let $\alpha_1 = C_s \nu^{-1} M_1$ and $\alpha_2 = C_s \kappa^{-1} M_2$. If $C_p^2 \nu^{-1} Ri,\ C_p^{1/2}(\alpha_2 + \alpha_1) < 1$, then the solutions to (9) are unique.

Remark. The constants α_1 and α_2 can be expressed in terms of Re, Pr, and Ra:

$$\alpha_1 = C_s\ Re^2 \|f\|_{V^*} + C_p^2\ Ra \|g\|_{D^*} \text{ and } \alpha_2 = C_s\ Re^2\ Pr^2 \|g\|_{D^*}.$$

2.2. The Picard iteration for the Boussinesq equations. We provide results for Picard applied to the Boussinesq equation (3) and include the proofs in the appendix for completeness. These results are similar to those found in [25, 31].

The weak formulations for Picard for the Boussinesq system takes the form: Find $(u^{k+1}, T^{k+1}) \in V \times D$ satisfying $\forall (v, w) \in V \times D$,

$$\begin{cases} b(u^k, u^{k+1}, v) + \nu(\nabla u^{k+1}, \nabla v) & = (f,v) + Ri(T^{k+1}\ \bar{e}_d, v), \\ \hat{b}(u^k, T^{k+1}, w) + \kappa(\nabla T^{k+1}, \nabla w) & = (g,w). \end{cases} \tag{12}$$

Note that the Picard iteration decouples the temperature equation and thus solving (12) is a two-step process where one first solves a scalar convection-diffusion problem and then an Oseen problem. Effective preconditioners for these linear systems exist in the literature [3, 16, 26, 6].

Lemma 2.3. Any solution to the Picard iteration for the Boussinesq equations satisfies the a priori estimate: for any $k = 1, 2...$,

$$\|\nabla T^k\| \leq M_2,$$
$$\|\nabla u^k\| \leq M_1.$$

Lemma 2.4. The Picard iteration (12) with problem data satisfying $\min\left\{1 - \nu^{-1}\frac{C_p^2 Ri}{2}, 1 - \kappa^{-1}\frac{C_p^2 Ri}{2}\right\} > 0$, admits a unique solution.

Lemma 2.5. Consider the Picard iteration (12) with problem data satisfying $C_p^2\nu^{-1}Ri < 1$ and
$C_p^{1/2}(\alpha_1+\alpha_2) < 1$. Then the iteration converges linearly with rate $C_p^{1/2}(\alpha_1+\alpha_2)$. In particular we have

$$\|\nabla(T-T^{k+1})\| \le C_p^{1/2}\alpha_2\|\nabla(u-u^k)\|,$$

and

$$\|\nabla(u-u^{k+1})\| \le C_p^{1/2}(\alpha_1+\alpha_2)\|\nabla(u-u^k)\|.$$

Remark. Recall that Lemma 2.2 gives the sufficient condition for uniqueness of Boussinesq solutions $C_p^2\nu^{-1}Ri,\ C_p^{1/2}(\alpha_1+\alpha_2) < 1$. This means that the conditions for convergence of Picard and the uniqueness of solutions to the Boussinesq equations are the same.

3. Finite Element Discretization

We now provide a finite element framework for Boussinesq. CDA as given herein acts on a coarse mesh, thus the results in the following section should be considered in a finite element space.

Let τ_h be a mesh on Ω with maximum element length h, and let $\mathbb{P}_k(\tau_H)$ denote the degree k continuous Lagrange finite element defined on τ_h. Then we define the finite element spaces $X_h = P_k(\tau_H)\cap X$ and $D_h = P_k(\tau_h)\cap D$. Then the weak formulation of CDA-Picard for the Boussinesq equations is given by: Given $f \in {X_h}^*$ and $g^* \in {D_h}^*$, find $(u,T) \in X_h \times D_h$ satisfying

$$\begin{cases} b(u^k,u^{k+1},v)+\nu(\nabla u^{k+1},\nabla v) & = (f,v)+Ri(T^{k+1}\,\bar{e}_d,v), \\ \hat{b}(u^k,T^{k+1},w)+\kappa(\nabla T^{k+1},\nabla w) & = (g,w). \end{cases} \tag{13}$$

We similarly define a coarse mesh $\tau_H(\Omega)$ with maximum element length $H \ge h$, and for simplicity we assume that the nodes of τ_H are also nodes of τ_h. Let $\mathbb{P}_k(\tau_H)$ denote the degree k continuous Lagrange finite element defined on τ_H. Then we define the finite element spaces $X_H = P_k(\tau_H)\cap X$ and $D_H = P_k(\tau_H)\cap D$. We define the interpolation operator I_H on $\tau_H(\Omega)$. We assume that I_H satisfies: $\exists$ a constant C_I independent of H satisfying

$$\|I_Hv-v\| \le C_IH\|\nabla v\| \ \ \forall v \in X_h \text{ and } D_h, \tag{14}$$

$$\|I_Hv\| \le C_I\|v\| \ \ \forall v \in X_h \text{ and } D_h. \tag{15}$$

In our numerical tests, we take I_H to be the L^2 projection onto $X_H = P_0(\tau_H)$, however all the presented analysis holds for any interpolant satisfying (14)-(15).

Remark. Throughout this paper, the constants $C_s,\ C_p$, and C_I are $O(1)$ constants.

4. Convergence of CDA-Picard for Boussinesq equations with (accurate) partial solution data

We now provide analytical results for CDA-Picard that uses accurate partial solution data. We begin by providing results for CDA-Picard when nudging both u and T, and then for nudging only u or T. To prove convergence, we will use the weighted H^1 norm

$$\|v\|_* := \sqrt{\frac{1}{4C_I^2H^2}\|v\|^2+\|\nabla v\|^2}.$$

This weighted H^1 norm naturally arises in the CDA-Picard analysis. For small H, the $*$-norm is essentially equivalent to the $L^2(\Omega)$ norm. Following [23], a modified analysis with additional assumptions could allow for L^2 norm estimates instead.

We have the following bounds on the $L^2(\Omega)$ norm.

Lemma 4.1. For any $v \in X_h, D_h$ all of the following hold:

$$\begin{aligned}\|v\|^{1/2}\|\nabla v\|^{1/2} &\leq (C_I H)^{1/2}\|v\|_*,\\ \|v\| &\leq C_p\|v\|_*,\\ \|v\| &\leq C_p^{1/2}(C_I H)^{1/2}\|v\|_*.\end{aligned}$$

Proof. Using Young's inequality and the definition of the $*$-norm we obtain

$$\|v\|^{1/2}\|\nabla v\|^{1/2} = \left(\frac{1}{4C_I H}\|v\|^2 + C_I H\|\nabla v\|^2\right)^{1/2} \leq (C_I H)^{1/2}\|v\|_*. \tag{16}$$

Using (16) and the Poincare inequality we get

$$\begin{aligned}\|v\| &\leq C_p\|\nabla v\| \leq C_p\|v\|_*,\\ \|v\| &= C_p^{1/2}\|v\|^{1/2}\|\nabla v\|^{1/2} \leq C_p^{1/2}(C_I H)^{1/2}\|v\|_*.\end{aligned}$$

□

We first assume that partial solution data is known at some set of points in Ω. Then the weak formulation of CDA-Picard for the Boussinesq equations (4) is given by: Given $f \in {X_h}^*$ and $g^* \in {D_h}^*$, find $(u, T) \in X_h \times D_h$ satisfying

$$\begin{cases} b(u^k, u^{k+1}, v) + \nu(\nabla u^{k+1}, \nabla v) & +\mu_1(I_H(u^{k+1} - u), I_H(v)) \\ & \quad = (f, v) + Ri(T^{k+1}\ \bar{e}_d, v), \\ \hat{b}(u^k, T^{k+1}, w) + \kappa(\nabla T^{k+1}, \nabla w) & +\mu_2(I_H(T^{k+1} - T), I_H(w)) \\ & \quad = (g, w). \end{cases} \tag{17}$$

Note that the term $\mu_1(I_H(u^{k+1} - u), I_H(v))$ does not follow the usual rules for the Galerkin weak formulation and may be considered a variational crime, if I_H is not the L^2 projection onto X_H. However, this results in μ not having an analytical upper bound. This lack of an upper bound for μ has been observed numerically in many CDA paper [28, 30, 34, 14, 24, 29, 13] therefore it is desirable to have analysis which reflects this.

4.1. Convergence of CDA-Picard nudging both u and T. We begin analyzing CDA-Picard (17) without noise when nudging both u and T, and then consider the case of nudging just u and just T which use similar techniques.

Remark. The small problem data conditions, $\alpha_1 + \alpha_2 < 1$, given in Section 2.2 and Section 1 is not required for the CDA theorems, and is therefore not assumed. The lemmas and conditions provided in Section 2.2 and Section 1 are included for completeness.

Theorem 4.1. *Let $\mu_1 \geq \frac{\nu}{4C_I^2H^2}$, $\mu_2 \geq \frac{\kappa}{4C_I^2H^2}$, $Ri\ \nu^{-1}C_p^2 < 1$, $C_p^{-1/2}\frac{4}{3}(C_I H)^{1/2} < 1$ and $\frac{4}{3}\sqrt{C_I H}(\alpha_1 + \alpha_2) < 1$. Then CDA-Picard converges linearly with rate at least $\frac{4}{3}\sqrt{C_I H}(\alpha_1 + \alpha_2)$:*

$$\|u - u^{k+1}\|_* + (1 - \frac{4}{3}Ri\ \nu^{-1}C_p^2)\|T - T^{k+1}\|_* \leq \frac{4}{3}(\alpha_1 + \alpha_2)(C_I H)^{1/2}\|u - u^k\|_*.$$

The conditions $\mu_1 \geq \frac{\nu}{4C_I^2H^2}$, $\mu_2 \geq \frac{\kappa}{4C_I^2H^2}$ should be interpreted as requiring μ_i be large enough for the given H. In practice this is usuallly done by taking μ_i to be large, such as $\mu_i = 1000$.

Remark. The condition $Ri\ \nu^{-1}C_p^2 < 1$ is the condition for well-posedness of the Boussinesq equations from Lemma 2.2. In the analysis, it appears together with the restriction
$C_p^{-1}\frac{4}{3}\sqrt{C_IH} \leq 1$. The analysis can be changed slightly to give the restriction $\frac{4}{3}Ri\ \nu^{-1}C_p^{3/2} < 1$ or the restriction $Ri\ \nu^{-1}C_p^{3/2} < 1$ and $\sqrt{C_IH} \leq \frac{3}{4}$.

Remark. Without CDA, Lemma 2.5 shows a sufficient condition for Picard convergence is
$C_p^{1/2}(\alpha_1 + \alpha_2) < 1$, and the convergence rate is $C_p^{1/2}(\alpha_1 + \alpha_2)$. Theorem 4.1 thus shows how CDA improves convergence rate and even enables convergence when Picard fails: the right hand side is scaled by $H^{\frac{1}{2}}$.

Proof. Let $e^{k+1} = u - u^{k+1}$ and $e_T^{k+1} = T - T^{k+1}$. We subtract (9) from (17) and set $v = e^{k+1}$ and $w = e_T^{k+1}$. Then we add and subtract terms to get

$$\begin{cases} b(e^k, e^{k+1}, e^{k+1}) + b(e^k, u, e^{k+1}) + b(u, e^{k+1}, e^{k+1}) \\ \qquad\qquad +\nu\|\nabla e^{k+1}\|^2 + \mu_1\|I_H(e^{k+1})\|^2 = Ri(e_T^{k+1}\ \bar{e}_d, e^{k+1}), \\ \hat{b}(u, e_T^{k+1}, e_T^{k+1}) + \hat{b}(e^k, e_T^{k+1}, e_T^{k+1}) + \hat{b}(e^k, T, e_T^{k+1}) \\ \qquad\qquad +\kappa\|\nabla e_T^{k+1}\|^2 + \mu_2\|I_H(e_T^{k+1})\|^2 = 0. \end{cases}$$

The skew symmetry of b and $\hat{b}$ vanishes four nonlinear terms yielding

$$\begin{cases} \nu\|\nabla e^{k+1}\|^2 + \mu_1\|I_H(e^{k+1})\|^2 & = Ri(e_T^{k+1}\ \bar{e}_d, e^{k+1}) - b(e^k, u, e^{k+1}), \\ \kappa\|\nabla e_T^{k+1}\|^2 + \mu_2\|I_H(e_T^{k+1})\|^2 & = -\hat{b}(e^k, T, e_T^{k+1}). \end{cases}$$

We next use Lemma 4.1, (5), and Lemma 2.1 to upper bound the right hand side as

$$\begin{cases} \nu\|\nabla e^{k+1}\|^2 + \mu_1\|I_H(e^{k+1})\|^2 & \leq RiC_p^{3/2}(C_IH)^{1/2}\|e_T^{k+1}\|_*\|e^{k+1}\|_* \\ & \qquad +\alpha_1\nu(C_IH)^{1/2}\|e^k\|_*\|e^{k+1}\|_*, \\ \kappa\|\nabla e_T^{k+1}\|^2 + \mu_2\|I_H(e_T^{k+1})\|^2 & \leq \alpha_2\kappa(C_IH)^{1/2}\|e^k\|_*\|e_T^{k+1}\|_*. \end{cases} \tag{18}$$

Next we lower bound the left hand sides using the interpolation bound and the triangle inequality via

$$\begin{cases} \nu\|\nabla e^{k+1}\|^2 + \mu_1\|I_H(e^{k+1})\|^2 & = \frac{\nu}{4}\|\nabla e^{k+1}\|^2 + \mu_1\|I_H(e^{k+1})\|^2 + \frac{3\nu}{4}\|\nabla e^{k+1}\|^2, \\ & \geq \frac{\nu}{4C_I^2H^2}\|e^{k+1} - I_H(e^{k+1})\|^2 + \mu_1\|I_H(e^{k+1})\|^2 \\ & \qquad +\frac{3\nu}{4}\|\nabla e^{k+1}\|^2, \\ & \geq \frac{\nu}{4C_I^2H^2}(\|e^{k+1} - I_H(e^{k+1})\|^2 + \|I_H(e^{k+1})\|^2) \\ & \qquad +\frac{3\nu}{4}\|\nabla e^{k+1}\|^2, \\ & \geq \frac{\nu}{4C_I^2H^2}\|e^{k+1}\|^2 + \frac{3\nu}{4}\|\nabla e^{k+1}\|^2, \\ & \geq \frac{3\nu}{4}\|e^{k+1}\|_*^2, \\ \kappa\|\nabla e_T^{k+1}\|^2 + \mu_2\|I_H(e_T^{k+1})\|^2 & = \frac{\kappa}{4}\|\nabla e_T^{k+1}\|^2 + \mu_2\|I_H(e_T^{k+1})\|^2 + \frac{3\kappa}{4}\|\nabla e_T^{k+1}\|^2, \\ & \geq \frac{\kappa}{4C_I^2H^2}\|e_T^{k+1} - I_H(e_T^{k+1})\|^2 + \mu_2\|I_H(e_T^{k+1})\|^2 \\ & \qquad +\frac{3\kappa}{4}\|\nabla e_T^{k+1}\|^2, \\ & \geq \frac{\kappa}{4C_I^2H^2}\|e_T^{k+1}\|^2 + \frac{3\kappa}{4}\|\nabla e_T^{k+1}\|^2, \\ & \geq \frac{3\kappa}{4}\|e_T^{k+1}\|_*^2, \end{cases}$$

by assumptions on μ_i being sufficiently large. Using this in (18) and simplifying yields

$$\begin{cases} \|e^{k+1}\|_* & \leq \frac{4}{3}\nu^{-1}RiC_p^{3/2}(C_IH)^{1/2}\|e_T^{k+1}\|_* + \frac{4}{3}\alpha_1 C_p(C_IH)^{1/2}\|e^k\|_*, \\ \|e_T^{k+1}\|_* & \leq \frac{4}{3}\alpha_2 C_p(C_IH)^{1/2}\|e^k\|_*. \end{cases}$$

Finally adding the equations gives the desired result. □

Theorem 4.2. *Let* $\mu_1 \geq \frac{\nu}{4C_I^2H^2}$, $\mu_2 \geq \frac{\kappa}{4C_I^2H^2}$, $Ri\ \nu^{-1}C_p^2 < 1$, $C_p^{-1/2}\frac{4}{3}(C_IH)^{1/2} < 1$ *and* $\frac{4}{3}\sqrt{C_IH}(\alpha_1+\alpha_2) < 1$. *Then the residual of CDA-Picard converges linearly with rate at least* $\frac{4}{3}\sqrt{C_IH}(\alpha_1+\alpha_2)$*:*

$$\|u^{k+1}-u^k\|_* + (1-\frac{4}{3}Ri\ \nu^{-1}C_p^2)\|T^{k+1}-T^k\|_* \leq \frac{4}{3}(\alpha_1+\alpha_2)(C_IH)^{1/2}\|u^k-u^{k-1}\|_*.$$

Remark. The conditions and rates for convergence of the error and residual for CDA-Picard are equivalent.

Proof. Let $e^{k+1} = u^k - u^{k+1}$ and $e_T^{k+1} = T^k - T^{k+1}$. We subtract (22) at time k and time $k+1$, add and subtract terms, and set $v = e^{k+1}$ and $w = e_T^{k+1}$ to get

$$\begin{cases} b(e^k,u^k,e^{k+1}) + b(u^k,e^{k+1},e^{k+1}) + \nu\|\nabla e^{k+1}\|^2 & +\mu_1\|I_H(e^{k+1})\|^2 \\ & = Ri(e_T^{k+1}\ \bar{e}_d, e^{k+1}), \\ \hat{b}(e^k,T^k,e_T^{k+1}) + \hat{b}(u^k,e_T^{k+1},e_T^{k+1}) + \kappa\|\nabla e_T^{k+1}\|^2 & +\mu_2\|I_H(e_T^{k+1})\|^2 \\ & = 0. \end{cases} \tag{19}$$

The skew symmetry of b and $\hat{b}$ vanishes nonlinear terms in (19) yielding,

$$\begin{cases} b(e^k,u^k,e^{k+1}) + \nu\|\nabla e^{k+1}\|^2 + \mu_1\|I_H(e^{k+1})\|^2 & = Ri(e_T^{k+1}\ \bar{e}_d, e^{k+1}), \\ \hat{b}(e^k,T^k,e_T^{k+1}) + \kappa\|\nabla e_T^{k+1}\|^2 + \mu_2\|I_H(e_T^{k+1})\|^2 & = 0. \end{cases}$$

The solutions u^k, T^k for $k = 1, ...$ satisfy the same stability bound as Lemma 2.3. We use this and (5) to obtain

$$\begin{cases} \nu\|\nabla e^{k+1}\|^2 + \mu_1\|I_H(e^{k+1})\|^2 & \leq RiC_p^{3/2}(C_IH)^{1/2}\|e_T^{k+1}\|_*\|e^{k+1}\|_* \\ & \quad +\alpha_1\nu(C_IH)^{1/2}\|e^k\|_*\|e^{k+1}\|_*, \\ \kappa\|\nabla e_T^{k+1}\|^2 + \mu_2\|I_H(e_T^{k+1})\|^2 & \leq \alpha_2\kappa(C_IH)^{1/2}\|e^k\|_*\|e_T^{k+1}\|_*. \end{cases}$$

We lower bound the left hand side analogously to Theorem 4.1,

$$\begin{cases} \|e^{k+1}\|_* & \leq \frac{4}{3}\nu^{-1}RiC_p^{3/2}(C_IH)^{1/2}\|e_T^{k+1}\|_* + \frac{4}{3}\alpha_1(C_IH)^{1/2}\|e^k\|_*, \\ \|e_T^{k+1}\|_* & \leq \frac{4}{3}\alpha_2(C_IH)^{1/2}\|e^k\|_*. \end{cases}$$

Finally we add the equations and simplify to get the desired results.

□

If we nudge just u then this is equivalent to setting $\mu_2 = 0$ in (17) which gives the following result.

Corollary 4.1. Let $\mu_1 \geq \frac{\nu}{4C_I^2H^2}$, $\mu_2 = 0$, $Ri\ \nu^{-1}C_p^2 < 1$, $C_p^{-1/2}\frac{4}{3}(C_IH)^{1/2} < 1$ and $(C_IH)^{1/2}(\frac{4}{3}\alpha_1 + C_p^{1/2}\alpha_2) < 1$. Then CDA-Picard converges linearly with rate at least $(C_IH)^{1/2}(\frac{4}{3}\alpha_1 + C_p^{1/2}\alpha_2)$:

$$\|u-u^{k+1}\|_* + (1-\frac{4}{3}\nu^{-1}RiC_p^{3/2})\|\nabla(T-T^{k+1})\| \leq \frac{4}{3}(C_IH)^{1/2}(\alpha_2+\alpha_1)\|u-u^k\|_*,$$

Proof. Let $e^{k+1} = u - u^{k+1}$ and $e_T^{k+1} = T - T^{k+1}$. We subtract (9) from (17) and set $v = e^{k+1}$ and $w = e_T^{k+1}$. Analagously to Theorem 4.1 we add and subtract terms and using the skew symmetry of b and $\hat{b}$ vanishes four nonlinear terms yielding

$$\begin{cases} \nu\|\nabla e^{k+1}\|^2 + \mu_1\|I_H(e^{k+1})\|^2 & = Ri(e_T^{k+1}\ \bar{e}_d, e^{k+1}) - b(e^k, u, e^{k+1}), \\ \kappa\|\nabla e_T^{k+1}\|^2 & = -\hat{b}(e^k, T, e_T^{k+1}). \end{cases}$$

We use Lemma 4.1, (5), Lemma 2.1 to upper bound the right hand side as

$$\begin{cases} \nu\|\nabla e^{k+1}\|^2 + \mu_1\|I_H(e^{k+1})\|^2 & \leq RiC_p^{3/2}(C_I H)^{1/2}\|\nabla e_T^{k+1}\|\|e^{k+1}\|_* \\ & \quad +\alpha_1\nu(C_I H)^{1/2}\|e^k\|_*\|e^{k+1}\|_*, \\ \kappa\|\nabla e_T^{k+1}\|^2 & \leq \alpha_2 C_p^{1/2}(C_I H)^{1/2}\kappa\|e^k\|_*\|\nabla e_T^{k+1}\|. \end{cases} \tag{20}$$

Next we lower bound the left hand sides using the interpolation bound and the triangle inequality as in Theorem 4.1 and use this in (20) to get

$$\begin{cases} \|e^{k+1}\|_* & \leq \frac{4}{3}\nu^{-1}RiC_p^{3/2}(C_I H)^{1/2}\|\nabla e_T^{k+1}\| + \frac{4}{3}\alpha_1(C_I H)^{1/2}\|e^k\|_*, \\ \|\nabla e_T^{k+1}\| & \leq \alpha_2 C_p^{1/2}(C_I H)^{1/2}\|e^k\|_* \end{cases}$$

Finally adding the equations gives the desired result. □

If we nudge just T then this is equivalent to setting $\mu_1 = 0$ in (17) which only gives the following result (where convergence is not improved for $H \to 0$).

Corollary 4.2. Let $\mu_1 = 0$, $\mu_2 \geq \frac{\nu}{4C_I^2 H^2}$, $Ri\ \nu^{-1}C_p^2 < 1$, and $(C_p^{1/2}\alpha_1 + \frac{4}{3}\sqrt{C_I H}\alpha_2) < 1$. Then CDA-Picard converges linearly with rate at least $(C_p^{1/2}\alpha_1 + \frac{4}{3}\sqrt{C_I H}\alpha_2)$:

$$\|\nabla(u-u^{k+1})\| + (1-\nu^{-1}RiC_p^2)\|T-T^{k+1}\|_* \leq (C_p^{1/2}\alpha_1 + \frac{4}{3}\alpha_2(C_I H)^{1/2})\|\nabla(u-u^k)\|.$$

Proof. Let $e^{k+1} = u - u^{k+1}$ and $e_T^{k+1} = T - T^{k+1}$. We subtract (9) from (17) and set $v = e^{k+1}$ and $w = e_T^{k+1}$. Analagously to Theorem 4.1 we add and subtract terms and using the skew symmetry of b and $\hat{b}$ vanishes 4 terms yielding

$$\begin{cases} \nu\|\nabla e^{k+1}\|^2 & = Ri(e_T^{k+1}\ \bar{e}_d, e^{k+1}) - b(e^k, u, e^{k+1}), \\ \kappa\|\nabla e_T^{k+1}\|^2 + \mu_2\|I_H(e_T^{k+1})\|^2 & = -\hat{b}(e^k, T, e_T^{k+1}). \end{cases}$$

We use Lemma 4.1, (5), (7), Lemma 2.1 to upper bound the right hand side as

$$\begin{cases} \nu\|\nabla e^{k+1}\|^2 + \mu_1\|I_H(e^{k+1})\|^2 & \leq RiC_p^2\|e_T^{k+1}\|_*\|\nabla e^{k+1}\| \\ & \quad +\alpha_1\nu C_p^{1/2}\|\nabla e^k\|\|\nabla e^{k+1}\|, \\ \kappa\|\nabla e_T^{k+1}\|^2 + \mu_2\|I_H(e_T^{k+1})\|^2 & \leq \alpha_2\kappa(C_I H)^{1/2}\|\nabla e^k\|\|e_T^{k+1}\|_*. \end{cases} \tag{21}$$

Next we lower bound the left hand sides using the interpolation bound and the triangle inequality analogously to Theorem 4.1 and use this in (21) to get

$$\begin{cases} \|\nabla e^{k+1}\| & \leq RiC_p^2\|e_T^{k+1}\|_* + \alpha_1 C_p^{1/2}\|\nabla e^k\|, \\ \|e_T^{k+1}\|_* & \leq \frac{4}{3}\alpha_2(C_I H)^{1/2}\|\nabla e^k\|. \end{cases}$$

Finally adding the equations gives the desired result. □

This corollary shows that nudging just T can improve the convergence rate (though less so than nudging just u) since it scales α_2. However, if α_1 is sufficiently large then nudging T may have little to no effect on convergence. We do note that this bound is not sharp.

Therefore, with accurate partial solution data there is a direct correlation between convergence, accuracy, and the amount of solution data collected H. Furthermore, CDA does not worsen the restrictions of Picard, so it can only improve convergence properties.

5. CDA-Picard for Boussinesq equation with noisy partial solution data

We suppose now that the partial solution data has noise (error) given by some $\epsilon(x)$, meaning that we have partial solution data given by $u+\epsilon_u$ and $T+\epsilon_T$ at the data points. Then the weak formulation of CDA-Picard for the Boussinesq equations (4) with noise is given by: Given $f \in X^*$ and $g^* \in D^*$, find $(u,T) \in X \times D$ satisfying

$$\begin{cases} b(u^k, u^{k+1}, v) + \nu(\nabla u^{k+1}, \nabla v) & +\mu_1(I_H(u^{k+1} - (u+\epsilon_u)), I_H(v)) \\ & \quad = (f,v) + Ri(T^{k+1}\ \bar{e}_d, v), \\ \hat{b}(u^k, T^{k+1}, w) + \kappa(\nabla T^{k+1}, \nabla w) & +\mu_2(I_H(T^{k+1} - (T+\epsilon_T)), I_H(w)) \\ & \quad = (g,w). \end{cases} \tag{22}$$

5.1. Convergence of CDA-Picard for Boussinesq equation with noisy partial solution data. We now we analyze CDA-Picard with noise (22) when nudging both u and T. We begin by analyzing the convergence of the residual and then the error.

Theorem 5.1. *Let* $\mu_1 \geq \frac{\nu}{4C_I^2H^2}$, $\mu_2 \geq \frac{\kappa}{4C_I^2H^2}$, $Ri\ \nu^{-1}C_p^2 < 1$, $C_p^{-1/2}\frac{4}{3}(C_IH)^{1/2} < 1$ *and* $\frac{4}{3}\sqrt{C_IH}(\alpha_1+\alpha_2) < 1$. *Then residual of CDA-Picard converges linearly with rate at least* $\frac{4}{3}\sqrt{C_IH}(\alpha_1+\alpha_2)$*:*

$$\|u^k - u^{k+1}\|_* + (1 - \frac{4}{3}\nu^{-1}RiC_p^{3/2}(C_IH)^{1/2})\|T^k - T^{k+1}\|_* \leq \frac{4}{3}(C_IH)^{1/2}(\alpha_1+\alpha_2)\|u^{k-1} - u^k\|_*.$$

Remark. The sufficient conditions for convergence of the residual for CDA with noisy partial solution data are the same as the sufficient conditions for convergence of error for CDA using accurate partial solution data.

Proof. This proof follows analogously to Theorem 4.2 because the terms $I_H(\epsilon_u)$ and $I_H(\epsilon_T)$ in (22) at time k and $k+1$ cancel when subtracting these two systems to form an error equation. □

Theorem 5.2. *Let* $\mu_1 \geq \frac{\nu}{4C_I^2H^2}$, $\mu_2 \geq \frac{\kappa}{4C_I^2H^2}$, $Ri\ \nu^{-1}C_p^2 < 1$, $\sqrt{C_IH} \leq \frac{3}{4}C_p$ *and* $\frac{4}{3}\sqrt{C_IH}(\alpha_1+\alpha_2) < 1$. *Then the error in CDA-Picard satisfies*

$$\begin{aligned} \|u - u^{k+1}\|_* + (1 - \frac{4}{3}\nu^{-1}RiC_p^{3/2}(C_IH)^{1/2})\|T - T^{k+1}\|_* \\ \leq (\frac{4}{3}(\alpha_1+\alpha_2)(C_IH)^{1/2})^{k+1}\|u - u^0\|_* \\ + C_I^2\frac{\frac{4}{3}(C_IH)^{1/2}}{1 - \frac{4}{3}(\alpha_1+\alpha_2)(C_IH)^{1/2}}(\mu_1\|\epsilon_u\| + \mu_2\|\epsilon_T\|). \end{aligned}$$

Proof. Let $e^{k+1} = u - u^{k+1}$ and $e_T^{k+1} = T - T^{k+1}$. We subtract (9) from (22) and set $v = e^{k+1}$ and $w = e_T^{k+1}$. Similarly to Theorem 4.1 we add and subtract terms and using the skew symmetry of b and $\hat{b}$ vanishes four terms, yielding

$$\begin{cases} \nu\|\nabla e^{k+1}\|^2 + \mu_1\|I_H(e^{k+1})\|^2 & = Ri(e_T^{k+1}\ \bar{e}_d, e^{k+1}) - b(e^k, u, e^{k+1}) \\ & \quad -\mu_1(I_H(\epsilon_u), I_H(e^{k+1})), \\ \kappa\|\nabla e_T^{k+1}\|^2 + \mu_2\|I_H(e_T^{k+1})\|^2 & = -\hat{b}(e^k, T, e_T^{k+1}) - \mu_2(I_H(\epsilon_T), I_H(e_T^{k+1})). \end{cases}$$

We use Lemma 4.1, (7), Lemma 2.1 to upper bound the right hand side as

$$\begin{cases} \nu\|\nabla e^{k+1}\|^2 + \mu_1\|I_H(e^{k+1})\|^2 & \leq RiC_p^{3/2}(C_IH)^{1/2}\|e_T^{k+1}\|_*\|e^{k+1}\|_* \\ & \quad +\alpha_1\nu(C_IH)^{1/2}\|e^k\|_*\|e^{k+1}\|_* \\ & \quad +\mu_1\|I_H(\epsilon_u)\|\|I_H(e^{k+1})\|, \\ \kappa\|\nabla e_T^{k+1}\|^2 + \mu_2\|I_H(e_T^{k+1})\|^2 & \leq \alpha_2\kappa(C_IH)^{1/2}\|e^k\|_*\|e_T^{k+1}\|_* \\ & \quad +\mu_2\|I_H(\epsilon_T)\|\|I_H(e_T^{k+1})\|. \end{cases} \tag{23}$$

Using the interpolation bound and Lemma 4.1 we can upper bound the terms

$$\|I_H(\epsilon_u)\|\|I_H(e^{k+1})\| \leq C_I^2(C_IH)^{1/2}\|\epsilon_u\|\|e^{k+1}\|_*,$$
$$\|I_H(\epsilon_T)\|\|I_H(e_T^{k+1})\| \leq C_I^2(C_IH)^{1/2}\|\epsilon_T\|\|e_T^{k+1}\|_*.$$

Combining this with (23) gives

$$\begin{cases} \nu\|\nabla e^{k+1}\|^2 + \mu_1\|I_H(e^{k+1})\|^2 & \leq RiC_p^{3/2}(C_IH)^{1/2}\|e_T^{k+1}\|_*\|e^{k+1}\|_* \\ & \quad +\alpha_1\nu(C_IH)^{1/2}\|e^k\|_*\|e^{k+1}\|_* \\ & \quad +\mu_1C_I^2(C_IH)^{1/2}\|\epsilon_u\|\|e^{k+1}\|_*, \\ \kappa\|\nabla e_T^{k+1}\|^2 + \mu_2\|I_H(e_T^{k+1})\|^2 & \leq \alpha_2\kappa(C_IH)^{1/2}\|e^k\|_*\|e_T^{k+1}\|_* \\ & \quad +\mu_2C_I^2(C_IH)^{1/2}\|\epsilon_T\|\|e_T^{k+1}\|_*. \end{cases} \tag{24}$$

Next we lower bound the left hand sides using the interpolation bound and the triangle inequality analogously to Theorem 4.1 and use this in (24) to get that

$$\begin{cases} \|e^{k+1}\|_* & \leq \frac{4}{3}\nu^{-1}RiC_p^{3/2}(C_IH)^{1/2}\|e_T^{k+1}\|_* + \frac{4}{3}\alpha_1(C_IH)^{1/2}\|e^k\|_* \\ & \quad +\frac{4}{3}\nu^{-1}\mu_1C_I^2(C_IH)^{1/2}\|\epsilon_u\|, \\ \|e_T^{k+1}\|_* & \leq \frac{4}{3}\alpha_2(C_IH)^{1/2}\|e^k\|_* + \frac{4}{3}\mu_2\kappa^{-1}C_I^2(C_IH)^{1/2}\|\epsilon_T\|. \end{cases}$$

Finally adding the equations gives

$$\|e^{k+1}\|_* + (1 - \frac{4}{3}\nu^{-1}RiC_p^{3/2}(C_IH)^{1/2})\|e_T^{k+1}\|_* \leq \frac{4}{3}(\alpha_1+\alpha_2)(C_IH)^{1/2}\|e^k\|_* + \frac{4}{3}C_I^2(C_IH)^{1/2}(\mu_1\nu^{-1}\|\epsilon_u\| + \mu_2\kappa^{-1}\|\epsilon_T\|).$$

Recall that $\frac{4}{3}(\alpha_1+\alpha_2)(C_IH)^{1/2} < 1$ therefore

$$\|e^{k+1}\|_* + (1 - \frac{4}{3}\nu^{-1}RiC_p^{3/2}(C_IH)^{1/2})\|e_T^{k+1}\|_* \leq (\frac{4}{3}(\alpha_1+\alpha_2)(C_IH)^{1/2})^{k+1}\|e^0\|_* + C_I^2\frac{\frac{4}{3}(C_IH)^{1/2}}{1-\frac{4}{3}(\alpha_1+\alpha_2)(C_IH)^{1/2}}(\mu_1\nu^{-1}\|\epsilon_u\| + \mu_2\kappa^{-1}\|\epsilon_T\|),$$

which completes the proof.

□

This result shows that the accuracy of the method depends on the noise of the partial solution data given by ϵ_u and ϵ_T. If $\epsilon_u = 0$ and $\epsilon_T = 0$ then the result reduces to Theorem 4.1. Furthermore, CDA-Picard with noise retains the improved convergence rate of $H^{\frac{1}{2}}(\alpha_1 + \alpha_2)$, but only converges up to the level of the noise.

6. Numerical Results

We now give numerical results for CDA-Picard for differentially heated cavity problems [5]. We consider (1) with $f = 0$, $g = 0$, $\nu = \kappa = 10^{-1}$, and Ri is varied which varies Ra for the problems. We will consider two test problems. For the first one, $\Omega = (0,1)^2 \subset \mathbb{R}^2$, with boundary conditions

$$\begin{cases} u & = 0 \ \text{ on } \partial\Omega, \\ T(0,y) & = 0, \\ T(1,y) & = 1, \\ \nabla T \cdot n & = 0, \ \text{on } y = 0, \ y = 1. \end{cases} \tag{25}$$

We study the convergence of CDA-Picard for varying physical parameters. For simplicity of presentation, we vary Ra only by fixing Pr and Re and varying Ri. For CDA we will use partial solution data with and without noise.

The discretization for the first test problem is as follows. Let τ_h be a barycenter refinement mesh of an $h = 1/64$ uniform triangulation, and note that all convergence results are comparable for other choices of h that we tested. Solutions to this system with $Ra = 1000000$ are shown in Figure 1. We define the spaces $X_h = \mathbb{P}_2(\tau_h) \cap X$, $Q_h = \mathbb{P}_1^{disc}(\tau_h) \cap Q$, and $D_h = \mathbb{P}_2(\tau_h) \cap D$. The spaces (X_h, Q_h) satisfy an LBB condition and provide divergence free velocity solutions [1], therefore all analytical results hold in the discrete spaces just as in (X, Q).

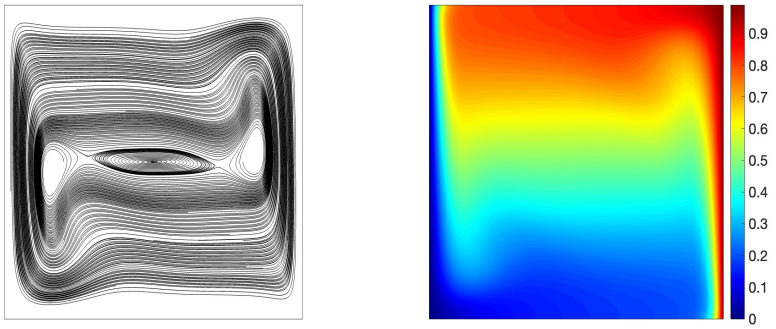

FIGURE 1. Shown above are the computed Boussinesq solution of the differentially heated cavity problem (25) for velocity streamlines (left) and temperature contours (right) for $Ra = 1000000$.

For our second test, we consider the unit cube $\Omega \subset \mathbb{R}^3$ with boundary conditions

$$\begin{cases} u & = 0 \ \text{ on } \partial\Omega, \\ T(0,y,z) & = 0, \\ T(1,y,z) & = 1, \\ \nabla T \cdot n & = 0, \ \text{on } y = 0, \ y = 1, \ z = 0, \ z = 1. \end{cases} \tag{26}$$

We again study the convergence of CDA-Picard for varying Ra, H, and μ. For CDA we will use partial solution data with and without noise. Solutions to this system with $Ra = 100000$ are shown in Figure 2.

For this problem, the mesh is created by first dividing the box into sub-rectangles using Chebychev points to weigh the degrees of freedom toward the boundary. Next, each box is split into 6 tetrahedra and finally, each of these tetrahedra are given a barycenter refinement resulting in 124554 degrees of freedom (dof) for velocity, 82320 dof for pressure, and 41518 dof for temperature. We define $X_h = \mathbb{P}_3(\tau_h) \cap X$, $Q_h = \mathbb{P}_2^{disc}(\tau_h) \cap Q$, and $D_h = \mathbb{P}_3(\tau_h) \cap D$. The spaces (X_h, Q_h) satisfy an LBB condition and provide divergence free velocity solutions [36], therefore all analytical results hold just as in (X, Q). We solve the velocity-pressure systems herein using the preconditioner from [3], which we implement with grad-div stabilization following [26].

For CDA, let τ_H be a mesh with max element diameter $h < H$ whose nodes represent collected partial solution data points. Let I_H be the L^2 projection operator from X onto X_H. This choice of projector allows for CDA implementation by algebraic nudging [34]. To implement data assimilation using algebraic nudging, we use a diagonal matrix with ones located at coarse mesh nodes and zeros elsewhere. The computation of this matrix is done offline i.e. prior to any iterations of the method. Furthermore since it is a very sparse matrix, the additional computational cost of incorporating this into the system is small. We will provide timings in one of the following sections to demonstrate this.

The analysis shows convergence in a weighted $H^1 \times H^1$ norm that depends on H which makes comparing the methods convergence at varying H difficult. Therefore, for simplicity for computations we use the B-norm

$$\|(u, T)\|_B := \sqrt{\nu\|\nabla u\|^2 + \kappa\|\nabla T\|^2}$$

in place of the $*$-norm, and note that in finite dimensional spaces all norms are equivalent. Thus we use the residual as the stopping criteria

$$\|(u^k, T^k) - (u^{k-1}, T^{k-1})\|_B = \sqrt{\nu\|\nabla(u^k - u^{k-1})\|^2 + \kappa\|\nabla(T^k - T^{k-1})\|^2} < 10^{-8}.$$

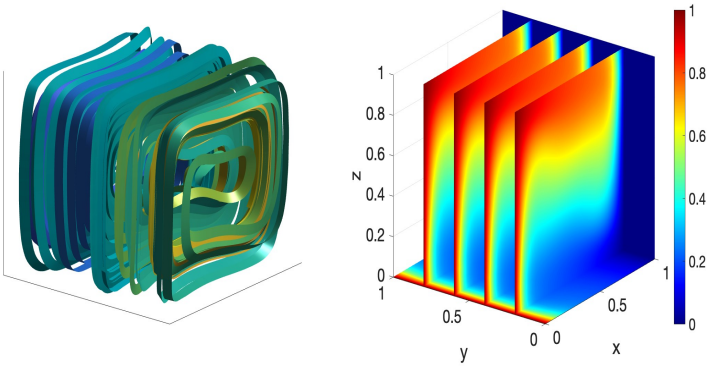

FIGURE 2. Shown above are the computed Boussinesq solution of the differentially heated cavity problem (26) for velocity streamlines (left) and temperature contours (right) for $Ra = 100000$.

6.1. CDA-Picard without noise. We begin with CDA-Picard without noise for the heated cavity problem in $2D$ (25) and give results for $Ra = 10000$ and 100000 with varying H and $\mu_1 = \mu_2 = 1000$. For comparison, we also run Picard without CDA. We note that we also performed this test with $\mu_1 = \mu_2 = 1$ and got very similar results for low Ra. However, $\mu_1 = \mu_2 = 1000$ performs better for higher Ra and is often necessary for convergence, hence we restrict our results to use only $\mu_1 = \mu_2 = 1000$.

First, for $Ra = 10000$ we see in Figure 3 (left) that Picard converges but it does so slowly. Immediately when we use CDA-Picard with $H = \frac{1}{4}$ we see a dramatic improvement in the convergence rate. The amount of partial solution data used is relatively small compared to the degrees of freedom (DoF) for the problem. CDA-Picard is further improved as H is decreased further. For $Ra = 100000$ in Figure 3 we see that CDA-Picard converges using $H = \frac{1}{8}, \frac{1}{16}$, and $\frac{1}{32}$ with iteration counts decreasing as H decreases.

We also compare the effect of varying μ for both $Ra = 10000$ and 100000 with $H = \frac{1}{8}$. In Figure 4, we see that for $Ra = 10000$, the convergence is improved similarly for any μ. For $Ra = 100000$, we see that as μ decreases the iteration count increases. Hence for CDA without noise, convergence is improved by larger H.

We now provide the timings for $Ra = 10000$. We provide the average computational cost per iteration of Picard or CDA-Picard. This is because the reduced iteration count for CDA-Picard will make the overall timings for CDA-Picard noticeable faster. For Picard (no data assimilation), one iteration takes 27.9 seconds. In table 2, we see that the timings of one iteration of CDA-Picard for vary H are all approximately the same at around 33 seconds. This is about 6 seconds slower than Picard. This additional cost doesn't scale with increasing or decreasing H. This is reasonable since the operations involving the implementation (the diagonal matrix with zeros and ones as entries) does have some overhead, but CDA-Picard is only 1.18 times slower.

We next provide some convergence results for CDA-Picard without noise for the heated cavity problem in $3D$ (26) for $Ra = 10000$ and 100000 with varying H. For comparison, we again run Picard without CDA and give its results in the figures. For $Ra = 10000$ in Figure 5 (left) we observe that Picard, without CDA, does not converge. In comparison, for CDA-Picard with $H = \frac{1}{5}$ we get convergence. The convergence rate is then improved as H decreases. For $Ra = 100000$ we see in Figure 5 (right) the same behavior with convergence beginning when $H = \frac{1}{15}$.

TABLE 1. Shown above are the maximal H for which CDA-Picard improves/enables convergence for $Ra = 10000,\ 100000$ and $\mu_1 = \mu_2 = 1000$.

Ra	Max H
10000	$\frac{1}{4}$
100000	$\frac{1}{8}$

6.2. $2D$ heated cavity with CDA using accurate partial solution data from only velocity and only temperature. Next we repeat the same test problem for $Ra = 10000$ and 100000 with $\mu_1 = 1000, \mu_2 = 0$ (nudge velocity only) and $\mu_1 = 0, \mu_2 = 1000$ (nudge temperature only). For $Ra = 10000$ with $\mu_1 = 1000$ and $\mu_2 = 0$ we see in Figure 6 (left) that CDA Picard converges for $H = \frac{1}{4},\ \frac{1}{8},\ \frac{1}{16},\ \frac{1}{32}$

TABLE 2. Shown above are timings per iteration for $Ra = 10000$ with varying H and $\mu_1 = \mu_2 = 1000$.

H	$\frac{1}{4}$	$\frac{1}{8}$	$\frac{1}{16}$	$\frac{1}{32}$
Seconds	33.16	33.09	33.61	32.8

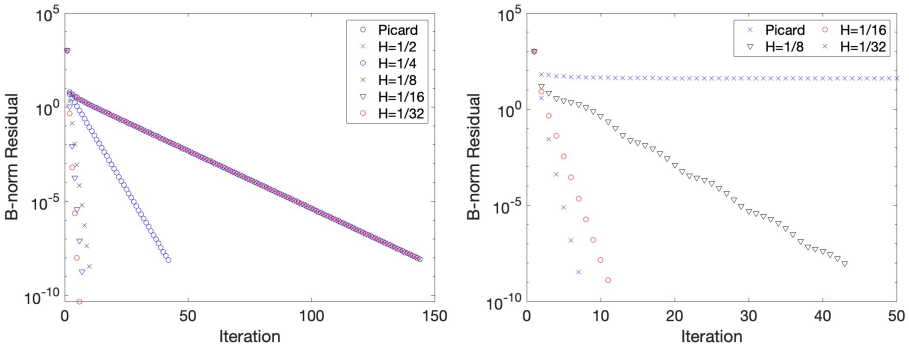

FIGURE 3. Shown above are the convergence plots for the $2D$ heated cavity problem for $Ra = 10000$ (left) and $Ra = 100000$ (right) with varying H for $\mu_1 = \mu_2 = 1000$.

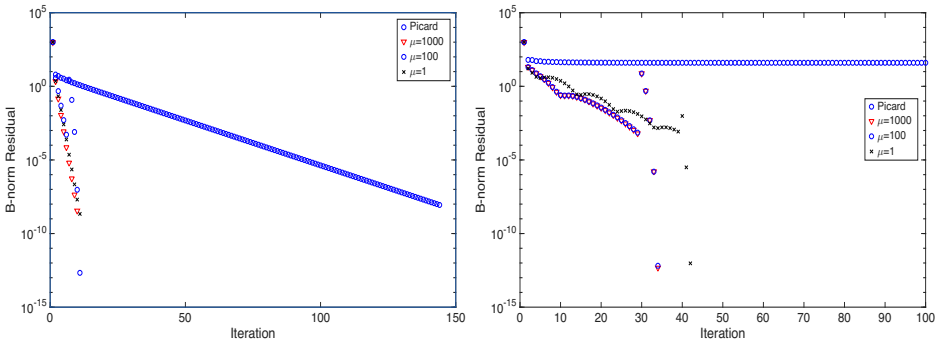

FIGURE 4. Shown above are the convergence plots for the $2D$ heated cavity problem for $Ra = 10000$ (left) and $Ra = 100000$ (right) with varying μ for $H = \frac{1}{8}$.

at approximately the same rate as $\mu_1 = \mu_2 = 1000$. This agrees with our theory. In comparison, for $\mu_1 = 0$ and $\mu_2 = 1000$ in Figure 7 (left) we see convergence for the same H but it converges slower. For $Ra = 100000$ with $\mu_1 = 1000$ and $\mu_2 = 0$ we see in Figure 6 (right) that CDA Picard converges for $H = \frac{1}{16}, \frac{1}{32}$ at a similar rate to $\mu_1 = \mu_2 = 1000$. In comparison, for $\mu_1 = 0$ and $\mu_2 = 1000$ in Figure 7 (right) we see convergence for the same H but it converges slower.

6.3. CDA-Picard with noise. We now consider CDA-Picard where the partial solution data has noise. Note that as μ_i increases the computed solution is increasingly nudged towards the given partial solution data. In the case of accurate partial solution data this is desirable but not necessarily for noisy partial solution data. Therefore, we consider the case when $\mu_1 = \mu_2 = 1$. We will first consider

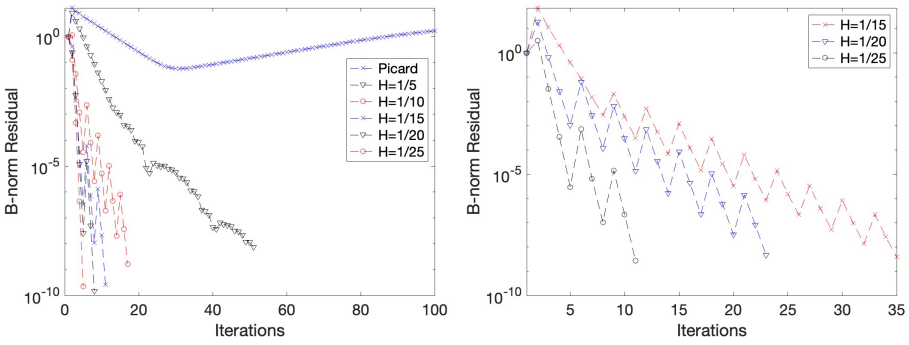

FIGURE 5. Shown above are the convergence plots for the $3D$ heated cavity problem for $Ra = 10000$ (left) and $Ra = 100000$ (right) with varying H for $\mu_1 = \mu_2 = 1000$.

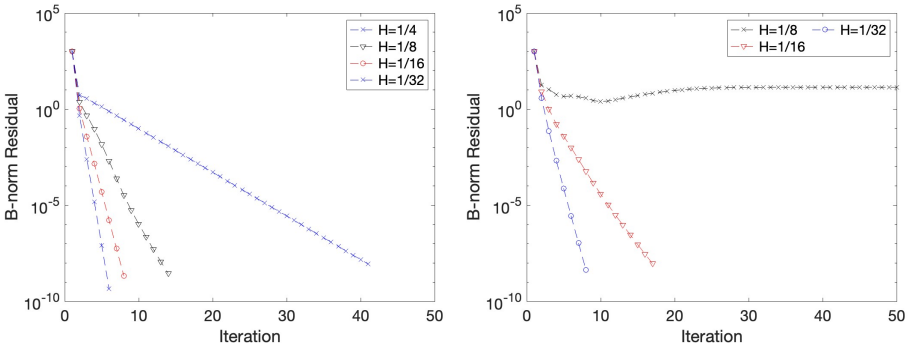

FIGURE 6. Shown above are the convergence plots for $Ra = 10000$ (left) and $Ra = 100000$ (right) with varying H for $\mu_1 = 1000, \mu_2 = 0$.

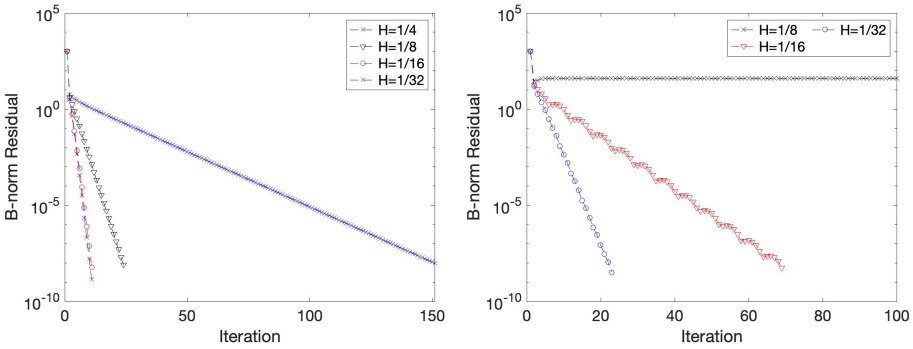

FIGURE 7. Shown above are the convergence plots for $Ra = 10000$ (left) and $Ra = 100000$ (right) with varying H for $\mu_1 = 0, \mu_2 = 1000$.

the $2D$ heated cavity problem for $Ra = 100000$ with varying H and noise satisfying $\|\epsilon_u\|, \|\epsilon_T\| = O(10^{-3})$. Noise is created at each point via scaling a uniform

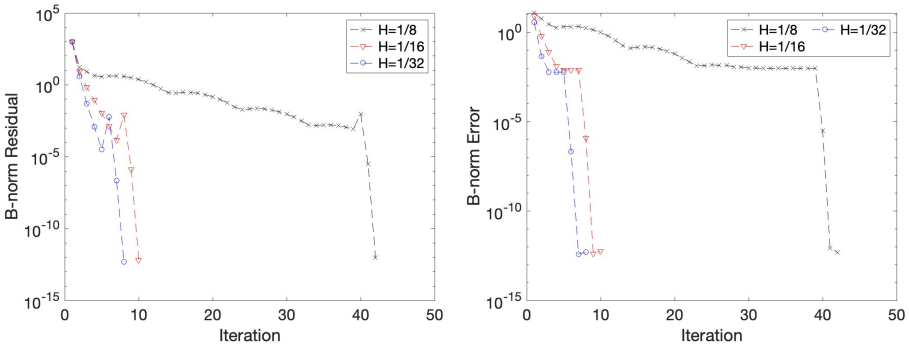

FIGURE 8. Shown above are the convergence plots for the residual (left) and error (right) for the heated cavity problem in $2D$ for $Ra = 100000$ with varying H, $\mu_1 = \mu_2 = 1$, and signal to noise ratio 10^{-3}.

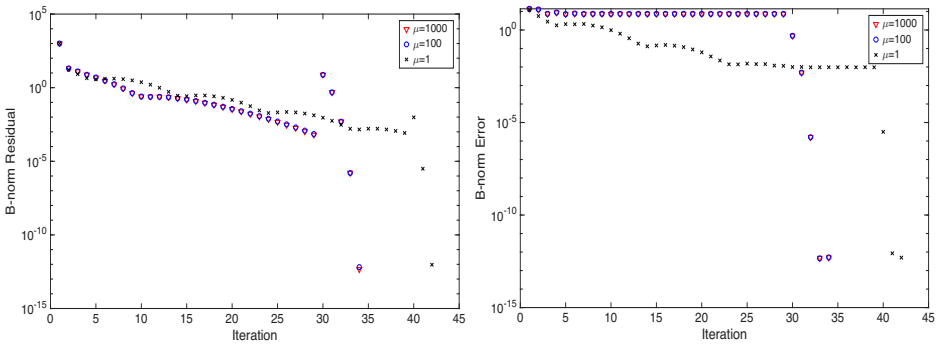

FIGURE 9. Shown above are the convergence plots for the residual (left) and error (right) for heated cavity problem in $2D$ for $Ra = 10000$ with varying μ, $H = \frac{1}{8}$, and signal to noise ratio 10^{-3}.

distribution on $[0, 1]$ by the max element and 10^{-3}, and then adding this to the accurate partial solution data. For this benchmark test we will provide both error and convergence plots.

Recall that for noisy partial solution data, our theory shows the error of the limit solution remains at the same order as the noise. Therefore in order to attain better accuracy using CDA with noisy partial solution data we must make an adjustment to the algorithm. When the residual of the iteration is less than 10^{-3}, CDA-Picard is turned off and the remaining solutions are found using the Newton iteration (without CDA). This is similar to the common method of using Picard to get an initial guess for Newton. However, recall that for these Ra, both Picard and Newton fail. Hence CDA-Picard *enables* Newton to be successful.

For $Ra = 100000$ in Figure 8 we see the residual steadily decreasing while using CDA-Picard. Concurrently, the error is decreasing until it is $O(10^{-3})$ where it levels off. When the solver is switched from CDA-Picard to Newton, the residual increases at the first step but immediately decreases quadratically to the desired accuracy. The error for the problem does the same and attains the desired accuracy.

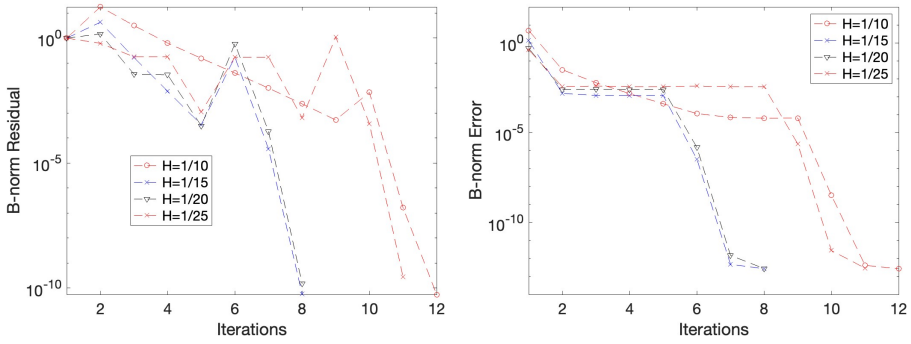

FIGURE 10. Shown above are the convergence plots for the residual (left) and error (right) for the heated cavity problem in $3D$ for $Ra = 100000$ with varying H, $\mu_1 = \mu_2 = 1$, and signal to noise ratio 10^{-3}.

We now repeat the same problem for heated cavity in $\mathbb{R}^3$ with $Ra = 100000$ with $\mu_1 = \mu_2 = 1$, varying H, and noise satisfying $\|\epsilon_u\|, \|\epsilon_T\| = O(10^{-3})$. Similarly to the $2D$ tests, we use CDA-Picard until the residual is less than 10^{-3} and then switch to Newton (without CDA). We see in Figure 10 (left) that for $Ra = 100000$ CDA-Picard converges with $H = \frac{1}{10}, \frac{1}{15}, \frac{1}{20}$, and $\frac{1}{25}$. When the iterative method changes from CDA-Picard to Newton there is an increase in the residual followed by a decrease for the remainder of the iterations. We also see in Figure 10 (right) that the errors for CDA-Picard level off at approximately $O(10^{-3})$ for each H, which is the same order as the noise.

We also compare the effect of varying μ_1, μ_2 for $Ra = 100000$ with $H = \frac{1}{8}$. In figure 9 (left), we see that the convergence of the residual is improved for any μ_1, μ_2, with greater improvement by the larger choices of μ_1, μ_2. However, the error is adversely affected by the larger μ_1, μ_2 with the error for $\mu_1, \mu_2 = 100, 1000$ being larger than the error for $\mu_1, \mu_2 = 1$. This matches the analysis given that the error term resulting from the noise depends on μ_1, μ_2. We also see in Figure 9 (right) that the error for $\mu_1, \mu_2 = 100, 1000$ levels off at $O(10^1)$. This is 4 orders of magnitude higher than the level off point for $\mu_1, \mu_2 = 1$. This further demonstrates the scaling by μ_1, μ_2 in the error term.

7. Conclusion

The residual and error of CDA-Picard for the Boussinesq equations converges at a faster rate compared to Picard, with speedup proportional to $H^{\frac{1}{2}}$ when nudging both velocity and temperature, or velocity only. Moreover, CDA enables convergence at higher Ra. The improved convergence using CDA with no noise on both u and T is demonstrated in both the $2D$ and $3D$ tests where convergence is observed for Ra that fail when using Picard alone. Furthermore the numerical tests in $2D$ for CDA with no noise on only u or only T also showed improved convergence.

When the partial solution data includes noise, the results are similar with the convergence rate of CDA-Picard containing a multiple of $H^{\frac{1}{2}}$. However, the accuracy of solutions to CDA-Picard is limited by the noise, as one would expect, due to an upper bound on the error containing a term which represents the accuracy of the partial solution data. The numerical tests for CDA with noise in both $2D$ and $3D$ demonstrated that the error when using noisy partial solution data is limited to

the accuracy of the partial solution data. This was resolved in the numerical tests (achieved convergence) by changing the iteration to Newton once a chosen residual accuracy is attained; this shows a possible a solution to the limited accuracy caused by noisy partial solution data.

Acknowledgments

This work was partially supported by the U.S. Department of Energy under award DE-SC0025292 and National Science Foundation grant DMS2152623.

Appendix

Lemma 7.1. Any solution to the Boussinesq equations (9) satisfies the a priori estimate

$$\|\nabla T\| \leq \|\nabla T\| \leq \kappa^{-1}\|g\|_{D^*} =: M_2, \tag{A.1}$$

$$\|\nabla u\| \leq \|\nabla u\| \leq \nu^{-1}\|f\|_{V^*} + RiC_p^2\nu^{-1}M_2 =: M_1. \tag{A.2}$$

Proof. We let $v = u$ and $w = T$ in (9) then using skew-symmetry gives us

$$\begin{cases} \nu\|\nabla u\|^2 = Ri((0\ T)^T, u) + (f, u), \\ \kappa\|\nabla T\|^2 = (g, T). \end{cases} \tag{A.3}$$

We upper bound the right hand side terms using the dual space norms, Cauchy-Schwarz, and Poincaré which yields

$$\begin{aligned} Ri((0\ T)^T, u) &\leq C_p^2 Ri\|\nabla T\|\|\nabla u\|, \\ (f, u) &\leq \|f\|_{V^*}\|\nabla u\|, \\ (g, T) &\leq \|g\|_{D^*}\|\nabla T\|. \end{aligned}$$

Using these bounds in (A.3) and reducing provides us with

$$\begin{cases} \|\nabla u\| \leq \nu^{-1}\|f\|_{V^*} + RiC_p^2\nu^{-1}\|\nabla T\|, \\ \|\nabla T\| \leq \kappa^{-1}\|g\|_{D^*}, \end{cases}$$

and using the second of these bounds in the first,

$$\|\nabla u\| \leq \nu^{-1}\|f\|_{V^*} + RiC_p^2\nu^{-1}\kappa^{-1}\|g\|_{D^*}.$$

This proves the result. □

Lemma 7.2. Let $\alpha_1 = C_s\nu^{-1}M_1$ and $\alpha_2 = C_s\kappa^{-1}M_2$. If $C_p^2\nu^{-1}Ri$, $C_p^{1/2}(\alpha_2 + \alpha_1) < 1$, then the solutions to (9) are unique.

Proof. Supposing two solutions (u_1, T_1) and (u_2, T_2) to (9) exists, and define $e_u = u_1 - u_2$ and $e_T = T_1 - T_2$. Now subtracting the systems with these two solutions gives $\forall v \in V, w \in D$,

$$\begin{cases} b(u_1, e_u, v) + b(e_u, u_2, v) + \nu(\nabla e_u, \nabla v) & = Ri((0\ e_T)^T, v), \\ \hat{b}(u_1, e_T, w) + \hat{b}(e_u, T_2, w) + \kappa(\nabla e_T, \nabla w) & = 0. \end{cases}$$

Taking $v = e_u$ and $w = e_T$ vanishes two nonlinear terms and leaves

$$\begin{cases} \nu\|\nabla e_u\|^2 & = Ri((0\ e_T)^T, e_u) - b(e_u, u_2, e_u) \\ & \leq C_p^2 Ri\|\nabla e_T\|\|\nabla e_u\| + C_pC_s\|\nabla e_u\|^2\|\nabla u_2\|, \\ \\ \kappa\|\nabla e_T\|^2 & = -\hat{b}(e_u, T_2, e_T) \\ & \leq C_p^{1/2}C_s\|\nabla T_2\|\|\nabla e_u\|\|\nabla e_T\|. \end{cases}$$

Next, using the bounds (A.2) and (A.1) and simplifying gives

$$\begin{cases} \|\nabla e_u\| & \leq C_p^2 \nu^{-1} Ri \|\nabla e_T\| + C_p^{1/2} \alpha_1 \|\nabla e_u\|, \\ \|\nabla e_T\| & \leq C_p^{1/2} \alpha_2 \|\nabla e_u\|. \end{cases} \tag{A.4}$$

Adding these and simplifying results in

$$(1 - C_p^{1/2}\alpha_1 - C_p^{1/2}\alpha_2)\|\nabla e_u\| + (1 - C_p^2 \nu^{-1} Ri)\|\nabla e_T\| \leq 0.$$

This provides the uniqueness of the velocity due to the assumption on the problem data. With this, uniqueness of the temperature follows immediately from the second bound in (A.4). □

Lemma 7.3. Any solution to the Picard iteration for the Boussinesq equations satisfies the a priori estimate: for any $k = 0, 1, 2...$,

$$\|\nabla T^{k+1}\| \leq M_2,$$
$$\|\nabla u^{k+1}\| \leq M_1,$$

Proof. These results are proved analogously to those of Lemma 2.1. □

Lemma 7.4. The Picard iteration (12) with problem data satisfying $\min\left\{1 - \nu^{-1}\frac{C_p^2 Ri}{2}, 1 - \kappa^{-1}\frac{C_p^2 Ri}{2}\right\} > 0$, admits a unique solution.

Remark. Note that (12) is linear. This combined with Lemma 2.3 immediately gives uniqueness. Furthermore, if the domain Ω is finite dimensional then this also implies existence of solutions.

Proof. Let $Y = V \times D$ and at iteration $k+1$ define $A : Y \times Y \to \mathbb{R}$ and $F : Y \to \mathbb{R}$ by

$$\begin{aligned} A((\hat{u}, \hat{T}), (v, w)) := b(u^k, \hat{u}, v) + \nu(\nabla \hat{u}, \nabla v) + \hat{b}(u^k, \hat{T}, w) + \kappa(\nabla \hat{T}, \nabla w) \\ - Ri((0\ \hat{T})^T, v), \\ F((v, w)) = (f, v) + (g, w), \end{aligned}$$

so that the Picard iteration is given by $A((\hat{u}, \hat{T}), (v, w)) = F((v, w))$. Consider $A((\hat{u}, \hat{T}), (v, w))$. Using (7), Cauchy-Schwarz, and Young's inequality we lower bound the equation as

$$\begin{aligned} A((\hat{u}, \hat{T}), (\hat{u}, \hat{T})) &= b(u^k, \hat{u}, \hat{u}) + \nu\|\nabla \hat{u}\|^2 + \hat{b}(u^k, \hat{T}, \hat{T}) + \kappa\|\nabla \hat{T}\|^2 - Ri((0\ \hat{T})^T, \hat{u}) \\ &\geq \nu\|\nabla \hat{u}\|^2 + \kappa\|\nabla \hat{T}\|^2 - \frac{C_p^2 Ri}{2}\|\nabla \hat{T}\|^2 - \frac{C_p^2 Ri}{2}\|\nabla \hat{u}\|^2 \\ &\geq \min\left\{\nu - \frac{C_p^2 Ri}{2}, \kappa - \frac{C_p^2 Ri}{2}\right\} \|(\hat{u}, \hat{T})\|_Y^2. \end{aligned}$$

Hence A is coercive. Continuity of A and F follow easily using the bounds and lemmas above. Thus Lax-Milgram applies and gives existence and uniqueness of (12).

□

Lemma 7.5. Consider the Picard iteration (12) with problem data satisfying $C_p^2 \nu^{-1} Ri < 1$ and $C_p^{1/2}(\alpha_1 + \alpha_2) < 1$. Then the iteration converges linearly with rate $C_p^{1/2}(\alpha_1 + \alpha_2)$. In particular we have

$$\|\nabla(T - T^{k+1})\| \leq C_p^{1/2}\alpha_2 \|\nabla(u - u^k)\|,$$

and

$$\|\nabla(u-u^{k+1})\| \leq C_p^{1/2}(\alpha_1+\alpha_2)\|\nabla(u-u^k)\|.$$

Proof. Let $e^{k+1}=u-u^{k+1}$ and $e_T^{k+1}=T-T^{k+1}$. We subtract (9) from (12) and choose $v=e^{k+1}$ and $w=e_T^{k+1}$. Using skew-symmetry , vanishes two non-linear terms and leaves the equality

$$\begin{cases} b(e^k,u,e^{k+1})+\nu\|\nabla e^{k+1}\|^2 & = Ri(e_T^{k+1}\ \bar{e_2},e^{k+1}), \\ \hat{b}(e^k,T,e_T^{k+1})+\kappa\|\nabla e_T^{k+1}\|^2 & = 0. \end{cases}$$

Next we use Cauchy-Schwarz, Poincaré, and (7) to upper bound these equations as

$$\begin{cases} \nu\|\nabla e^{k+1}\|^2 & \leq C_p^2 Ri\|\nabla e_T^{k+1}\|\|\nabla e^{k+1}\|+C_pC_s\|\nabla e^k\|\|\nabla u\|\|\nabla e^{k+1}\|, \\ \kappa\|\nabla e_T^{k+1}\|^2 & \leq C_pC_s\|\nabla e^k\|\|\nabla T\|\|\nabla e_T^{k+1}\|. \end{cases}$$

Then we reduce and apply Lemma 2.1 to get

$$\begin{cases} \|\nabla e^{k+1}\| & \leq C_p^2\nu^{-1}Ri\|\nabla e_T^{k+1}\|+C_p\alpha_1\|\nabla e^k\|, \\ \|\nabla e_T^{k+1}\| & \leq C_p\alpha_2\|\nabla e^k\|. \end{cases}$$

this gives the bound

$$\|\nabla e_T^{k+1}\| \leq C_p\alpha_2\|\nabla e^k\|,$$

Adding the equations and reducing gives

$$\|\nabla e^{k+1}\|+(1-C_p^2 Ri\ \nu^{-1})\|\nabla e_T^{k+1}\|^2 \leq C_p(\alpha_1+\alpha_2)\|\nabla e^k\|.$$

Finally, using the assumptions on the problem data finishes the proof. □

References

[1] D. Arnold and J. Qin. Quadratic velocity/linear pressure Stokes elements. In R. Vichnevetsky, D. Knight, and G. Richter, editors, *Advances in Computer Methods for Partial Differential Equations VII*, pages 28–34. IMACS, 1992.

[2] A. Azouani, E. Olson, and E. S. Titi. Continuous data assimilation using general interpolant observables. *Journal of Nonlinear Science*, 24:277–304, 2014.

[3] M. Benzi and M. Olshanskii. An augmented Lagrangian-based approach to the Oseen problem. *SIAM J. Sci. Comput.*, 28:2095–2113, 2006.

[4] H. Bessaih, E. Olson, and E. S. Titi. Continuous data assimilation with stochastically noisy data. *Nonlinearity*, 28(3):729–753, 2015.

[5] J. Boland and W. Layton. Error analysis for finite elements for steady natural convection problems. *Numerical Functional Analysis and Optimization*, 11:449–483, 1990.

[6] S. Börm and S. Le Borne. *H*-LU factorization in preconditioners for augmented Lagrangian and grad-div stabilized saddle point systems. *International Journal for Numerical Methods in Fluids*, 68:83–98, 2012.

[7] Y. Cao, A. Giorgini, M. Jolly, and A. Pakzad. Continuous data assimilation for the 3D Ladyzhenskaya model: analysis and computations. *Nonlinear Anal. Real World Appl.*, 68(103659):1–29, 2022.

[8] E. Carlson, J. Hudson, and A. Larios. Parameter recovery for the 2 dimensional Navier-Stokes equations via continuous data assimilation. *SIAM Journal on Scientific Computing*, 42(1):A250–A270, 2020.

[9] E. Carlson, J. Hudson, A. Larios, V. R. Martinez, E. Ng, and J. P. Whitehead. Dynamically learning the parameters of a chaotic system using partial observations. *DCDS*, 32(8):3809–3839, 2022.

[10] E. Celik and E. Olson. Data assimilation using time-delay nudging in the presence of Gaussian noise. *Journal of Nonlinear Science*, 2023.

[11] A. Cibik, R. Fang, W. Layton, and F. Siddiqua. Adaptive parameter selection in nudging based data assimilation. *Computer Methods in Applied Mechanics and Engineering*, 433, 2025.

[12] A. Cibik and S. Kaya. A projection-based stabilized finite element method for steady-state natural convection problem. *Journal of Mathematical Analysis and Applications*, 381:469–484, 2011.

[13] A. Diegel, X. Li, and L. Rebholz. Analysis of continuous data assimilation with large (or even infinite) nudging parameters. *Journal of Computational and Applied Mathematics*, 456, 2025.

[14] A. E. Diegel and L. G. Rebholz. Continuous data assimilation and long-time accuracy in a C^0 interior penalty method for the Cahn-Hilliard equation. *Applied Mathematics and Computation*, 424:127042, 2022.

[15] A. Larios E. Carlson. Sensitivity analysis for the 2D Navier-Stokes equations with applications to continuous data assimilation. *J Nonlinear Sci*, 31(84), 2021.

[16] H. Elman, D. Silvester, and A. Wathen. *Finite Elements and Fast Iterative Solvers with applications in incompressible fluid dynamics*. Numerical Mathematics and Scientific Computation. Oxford University Press, Oxford, 2014.

[17] A. Farhat, M. S. Jolly, and E. S. Titi. Continuous data assimilation for the 2D Bénard convection through velocity measurements alone. *Phys. D*, 303:59–66, 2015.

[18] A. Farhat, E. Lunasin, and Edriss E. Titi. Data assimilation algorithm for 3D Bénard convection in porous media employing only temperature measurements. *J. Math. Anal. Appl.*, 438(1):492–506, 2016.

[19] A. Farhat, E. Lunasin, and E. Titi. Abridged continuous data assimilation for the 2D Navier–Stokes equations utilizing measurements of only one component of the velocity field. *J. Math. Fluid Mech.*, 18(1):1–23, 2016.

[20] A. Farhat, E. Lunasin, and E. S. Titi. On the Charney conjecture of data assimilation employing temperature measurements alone: The paradigm of 3D planetary geostrophic model. *Mathematics of Climate and Weather Forecasting*, 2(1), 2016.

[21] A. Farhat, E. Lunasin, and E. S. Titi. *A Data Assimilation Algorithm: the Paradigm of the 3D Leray-α Model of Turbulence*, pages 253–273. London Mathematical Society Lecture Note Series. Cambridge University Press, 2019.

[22] C. Foias, C. F. Mondaini, and E. S. Titi. A discrete data assimilation scheme for the solutions of the two-dimensional Navier-Stokes equations and their statistics. *SIAM J. Appl. Dyn. Syst.*, 15(4):2109–2142, 2016.

[23] B. Garcia-Archilla, X. Li, J. Novo, and L. Rebholz. Enhancing nonlinear solvers for the Navier-Stokes equations with continuous (noisy) data assimilation. *Computer Methods in Applied Mechanics and Engineering*, 424, 2024.

[24] B. Garcia-Archilla, J. Novo, and E. Titi. Uniform in time error estimates for a finite element method applied to a downscaling data assimilation algorithm. *SIAM Journal on Numerical Analysis*, 58:410–429, 2020.

[25] E. Hawkins. Anderson-Picard based nonlinear preconditioning of the Newton iteration for non-isothermal flow simulations. *arxiv:2408.16872*, 2024.

[26] T. Heister and G. Rapin. Efficient augmented Lagrangian-type preconditioning for the Oseen problem using grad-div stabilization. *Int. J. Numer. Meth. Fluids*, 71:118–134, 2013.

[27] K. Huang, B. Mohanty, F. Leij, and M. Genuchten. Solution of the nonlinear transport equation using modified Picard iteration. *Advances in Water Resources*, 21:237–249, 1996.

[28] A. H. Ibdah, C. F. Mondaini, and E. S. Titi. Fully discrete numerical schemes of a data assimilation algorithm: uniform-in-time error estimates. *IMA Journal of Numerical Analysis*, 40(4):2584–2625, 11 2019.

[29] M.S. Jolly and A. Pakzad. Data assimilation with higher order finite element interpolants. *International J. for Num. Methods*, 95:472–490, 2023.

[30] A. Larios, L. Rebholz, and C. Zerfas. Global in time stability and accuracy of IMEX-FEM data assimilation schemes for Navier-Stokes equations. *Computer Methods in Applied Mechanics and Engineering*, 345:1077–1093, 2019.

[31] W. Layton. *An Introduction to the Numerical Analysis of Viscous Incompressible Flows*. SIAM, Philadelphia, 2008.

[32] P. C. Di Leoni, A. Mazzino, and L. Biferale. Synchronization to big data: nudging the Navier-Stokes equations for data assimilation of turbulent flows. *Physical Review X*, 10(011023), 2020.

[33] S. Pollock and L. Rebholz. *Anderson Acceleration for Numerical PDEs*. Society for Industrial and Applied Mathematics, Philadelphia, 2025.

[34] L. G. Rebholz and C. Zerfas. Simple and efficient continuous data assimilation of evolution equations via algebraic nudging. *Numerical Methods for Partial Differential Equations*, 37(3):2588–2612, 2021.
[35] L. Xuejian, L. Rebholz, D. Vargun, and E. Hawkins. Accelerating and enabling convergence of nonlinear solvers for Navier-Stokes equations by continuous data assimilation. *Computer Methods in Applied Mechanincs and Engineering*, 416, 2023.
[36] S. Zhang. Divergence-free finite elements on tetrahedral grids for $k \geq 6$. *Math. Comp.*, 80(274):669–695, 2011.
[37] T. Zhong, J. Yuan, and Z. Shi. Decoupled two grid finite element method for the time dependent natural convection problem I: spatial discretization. *Numerical Methods for Partial Differential Equations*, 31:2135–2168, 2015.

School of Mathematical and Statistical Sciences, Clemson University, Clemson, SC 29634, USA
E-mail: evhawki@clemson.edu